4.3.6 [Case 6] Test: Random initial pattern, discarding the nonlinear contribution

A test case was run eliminating the nonlinear contribution to the anisotropic DKS equation. Here, we turned off the two coefficients related to the nonlinear terms and analyzed the evolution of the system in a random initial pattern. Figure 47 presents the time evolution of the L_1 norm rate of variation, internal iterations, and maximum height modulus $|\bar{h}_n|$, and from Figure 48 to Figure 51 we can follow the morphology development. Without the stabilization by nonlinear terms, the height values keep continuously growing and changing with a disorganized nonsteady cellular-like structure. The maximum height modulus presents a exponential behavior in time, which is plotted as linear with the logarithmic $y - axis$.

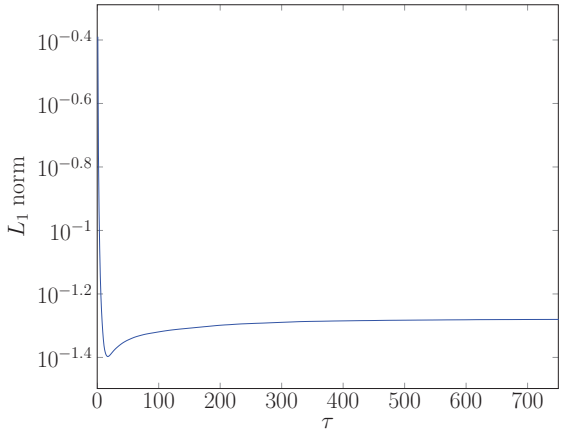

(a) L_1 norm rate of variation

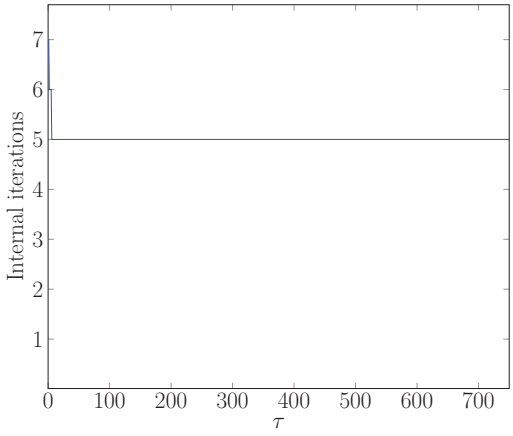

(b) Internal iterations

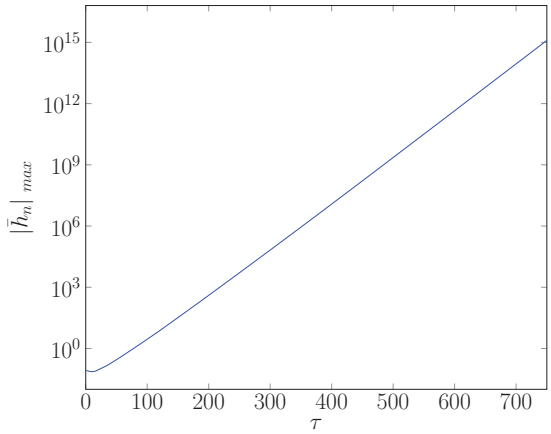

(c) Maximum $|\bar{h}_n|$

Figure 47: L_1 norm, internal iterations and maximum values for $\bar{h}_n$ as a function of time τ,for a random initial pattern, $\Delta\tau = 0.1$, $\Delta X = \Delta Y = 2$, on a 256×256 nodes domain. Nonlinear coefficients are discarded.

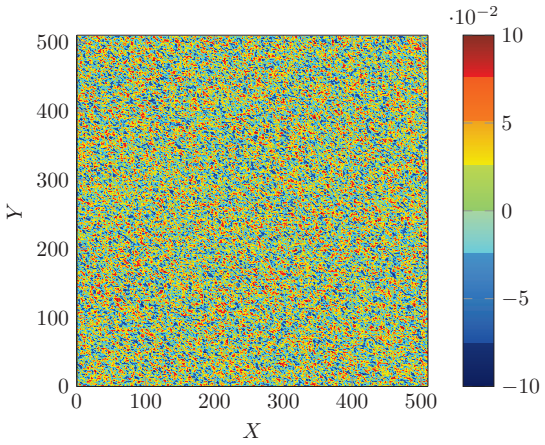

Figure 48: Surface height value $\bar{h}_n$ for $\tau = 0$.

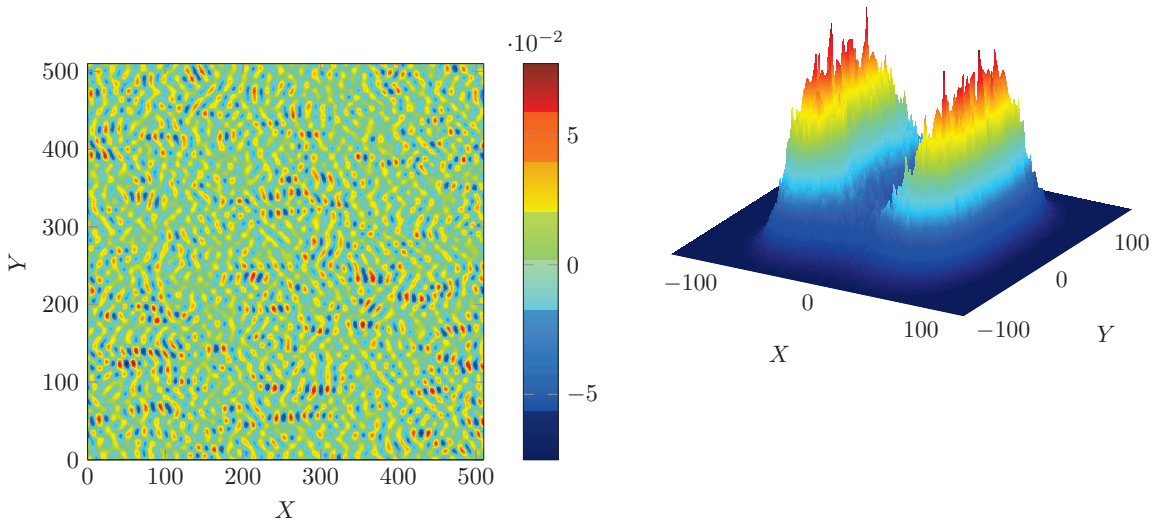

Figure 49: Surface height values $\bar{h}_n$ and their respective Fourier Transform for $\tau = 15$.

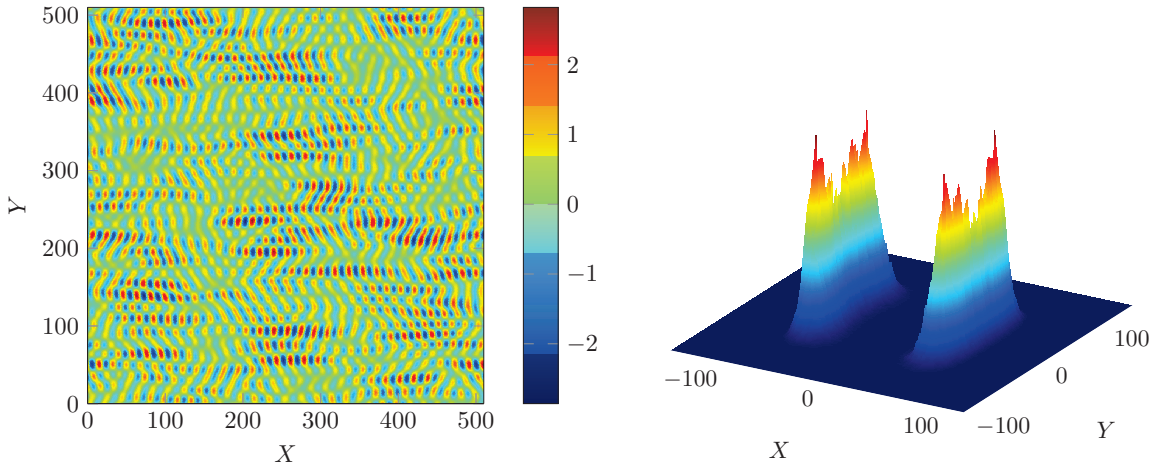

Figure 50: Surface height values $\bar{h}_n$ and their respective Fourier Transform for $\tau = 100$.

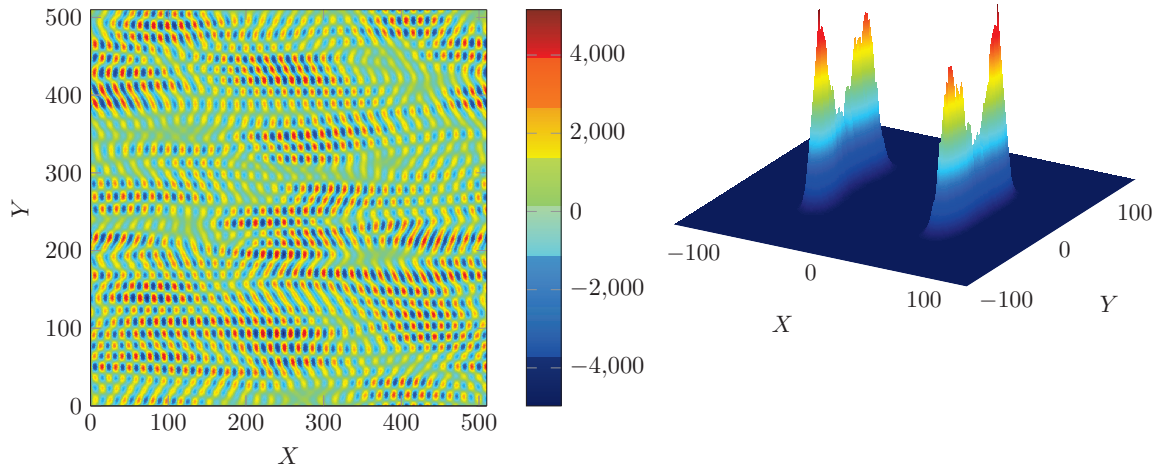

Figure 51: Surface height values $\bar{h}_n$ and their respective Fourier Transform for $\tau = 250$.

4.3.7 [Case 7] Spatial resolution test, 18 points per critical wavelength: Initial pattern with $\vec{q} = q_0\vec{1}_X$, 2 wavelengths

The seventh simulation uses the same initial pattern as Case 2, but increases the number of points per critical wavelength to 18 ($\Delta X = \Delta Y = 1.0$). Although the stability tests have not accused the spatial resolution of Case 2 as a potential problem, we insisted in the matter with this final test. Our aim was to study if the remaining defects of Case 2 had any relation to the spatial resolution. Figure 52 contains the usual information about evolution in time of the L_1 norm rate of variation, internal iterations, and maximum height modulus, while between Figure 53 and Figure 58 we have the surface morphology in time, alongside the FFT for each state.

Our first perception was that the spatial resolution really mattered this time, since we got results astonishingly different from Case 2, with a defectless final nanohole pattern. However, this conclusion was a mistake, and it was owning to the initial conditions. Although both cases start with 2 wavelengths with a monomodal $\vec{1}_X$ pattern, the wavenumber for Case 7 was slightly different than each was in Case 2. Thereafter, we repeated the simulation with $q_0 = 2.4544 \cdot 10^{-2}$, just like Case 2, and the exact same results were obtained. The sensibility towards the initial condition is the key to understand such distinct results.

Even though the results of Case 7 are related to an initial pattern with a wavenumber marginally different from Case 2, we still acquired an interesting material to analyze. From $\tau =$

0 to $\tau = 400$, it is possible to follow the nanostructuration of a 1D pattern with a wavenumber near q_c, as we have seen for Case 1. Based on the L_1 curve and on the maximum height modulus, one could think that a steady state was already reached around $\tau = 2,000$, since $\bar{h}_n$ stabilized in a minimum of -0.42, and the pattern calmed down (see the continuous and pronounced fall of L_1). Nonetheless, after $\tau = 2,000$, the hexagonal modes emerge, and the 1D structure destabilizes, as seen in Figure 57 for $\tau = 2,500$. The L_1 curve rapidly ascends to its peek and then falls down, as the structure reorganizes and stabilizes with the new hexagonal pattern. A defectless nanohole pattern is attained for the steady state, with a minimum height frozen at -0.8.

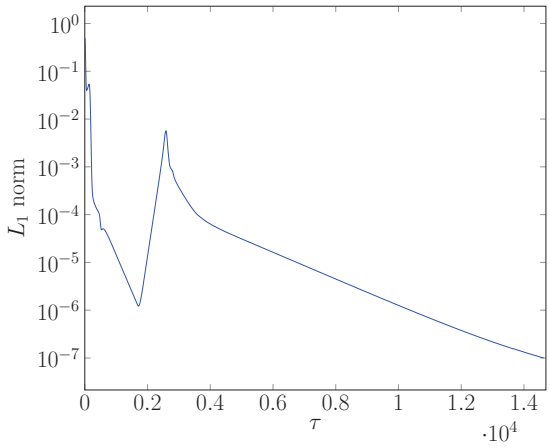

(a) L_1 norm rate of variation

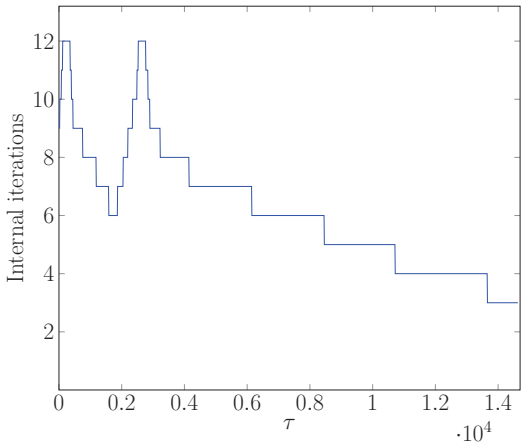

(b) Internal iterations

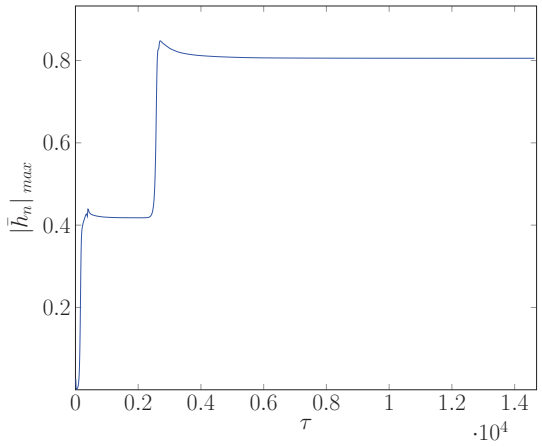

(c) Maximum $|\bar{h}_n|$

Figure 52: L_1 norm, internal iterations and maximum values for $\bar{h}_n$ as a function of time τ, for an initial pattern with $\vec{q} = q_0\vec{1}_X$ (inside the stable domain), $\Delta\tau = 0.1$, $\Delta X = \Delta Y = 1$, on a 512×512 nodes domain

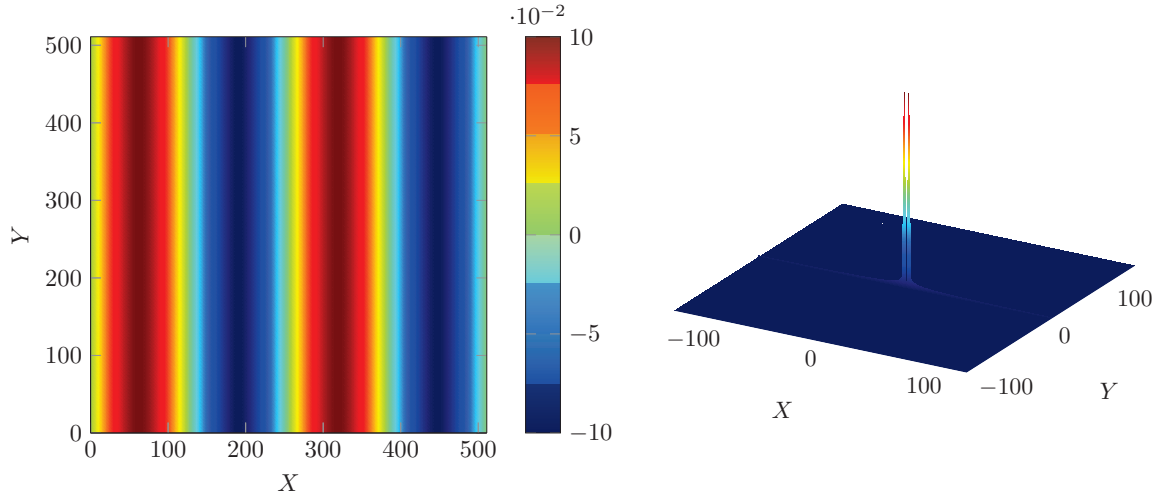

Figure 53: Surface height values $\bar{h}_n$ and their respective Fourier Transform for $\tau = 0$ (initial monomodal pattern with $\vec{q} = q_o \vec{1}_X$).

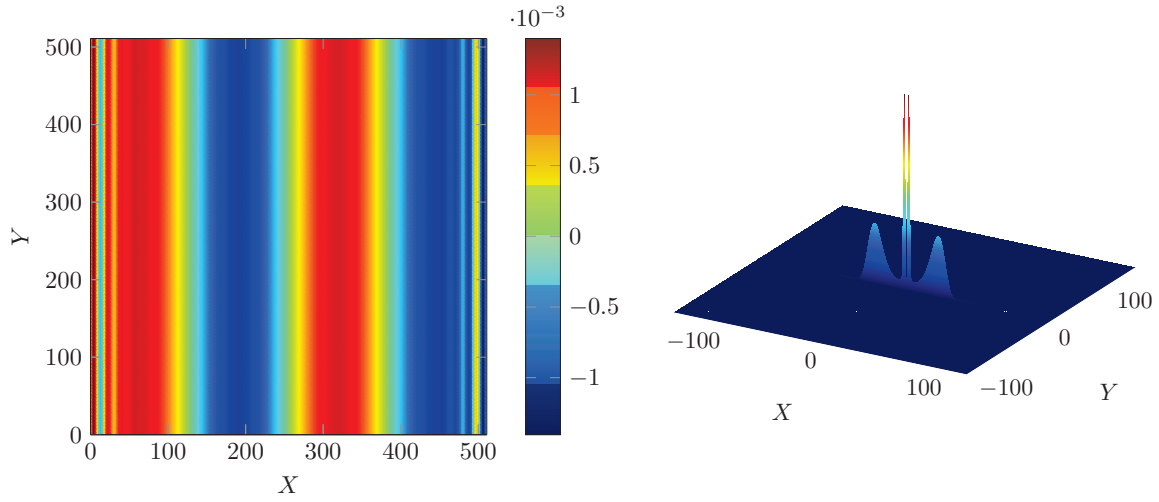

Figure 54: Surface height values $\bar{h}_n$ and their respective Fourier Transform for $\tau = 30$.

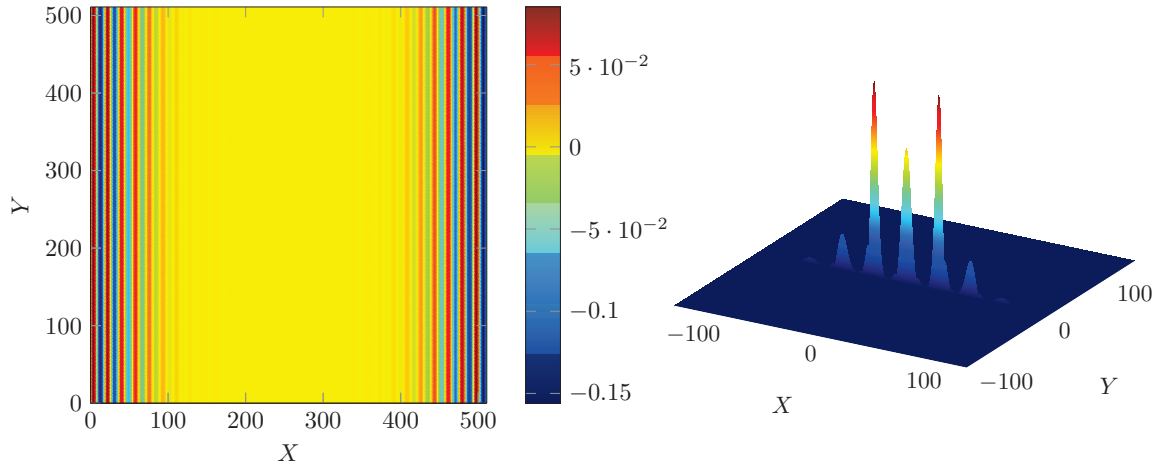

Figure 55: Surface height values $\bar{h}_n$ and their respective Fourier Transform for $\tau = 150$.

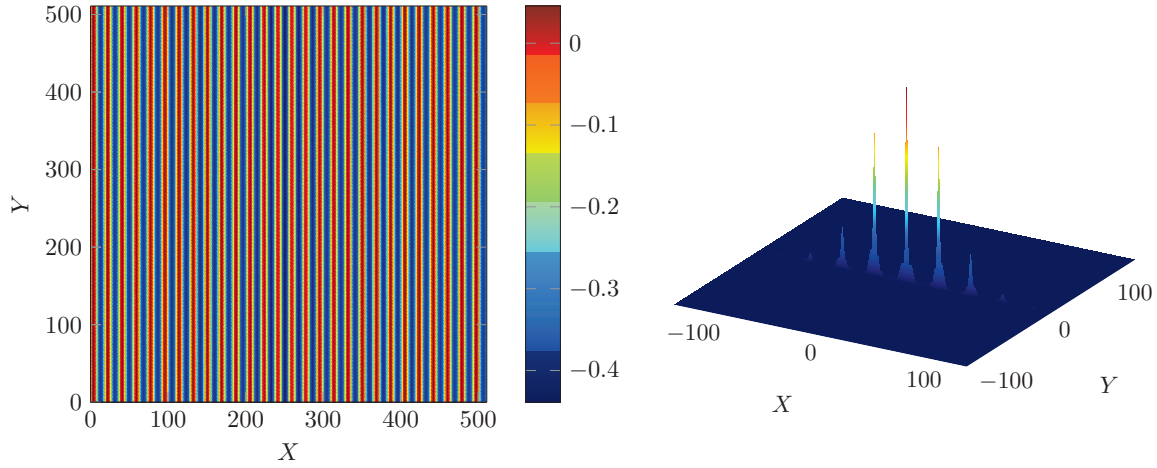

Figure 56: Surface height values $\bar{h}_n$ and their respective Fourier Transform for $\tau = 400$.

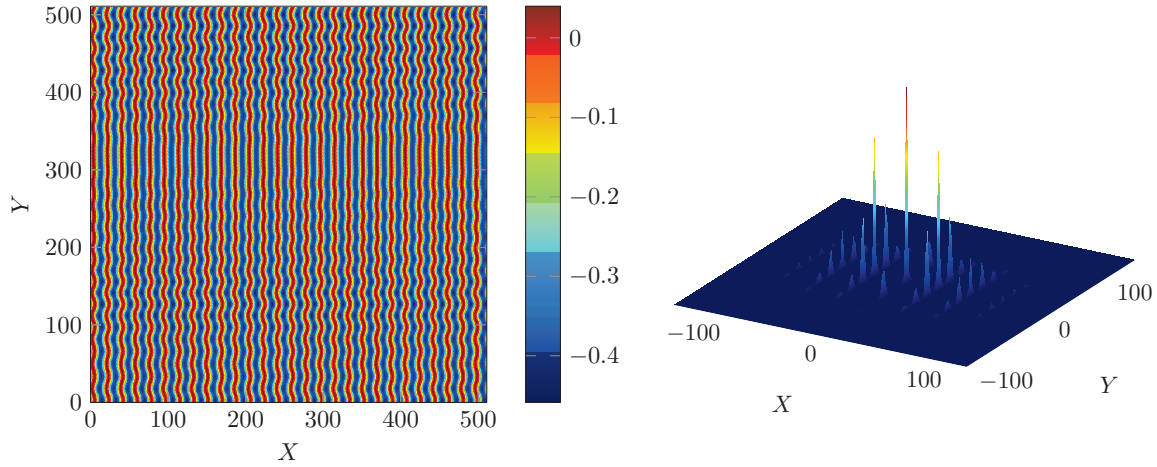

Figure 57: Surface height values $\bar{h}_n$ and their respective Fourier Transform for $\tau = 2,500$.

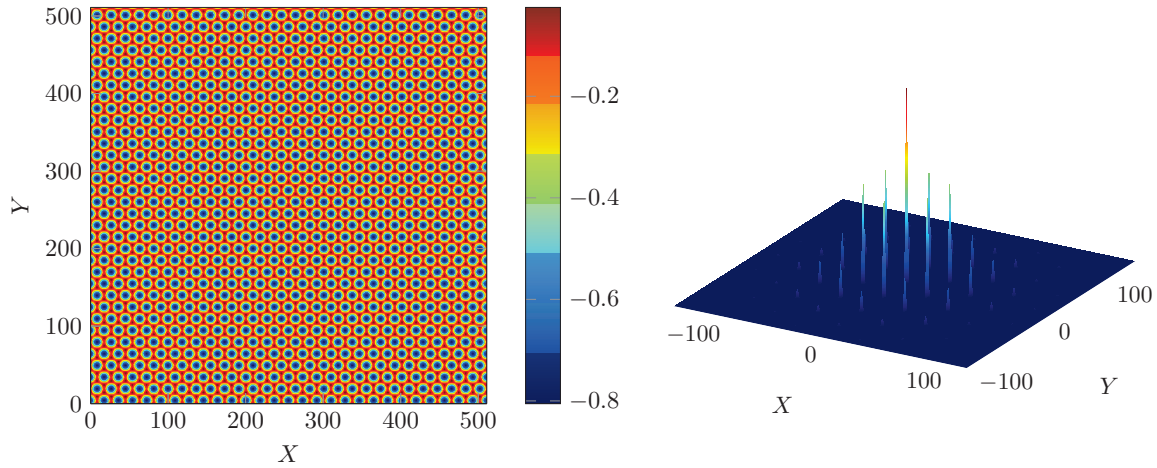

Figure 58: Surface height values $\bar{h}_n$ and their respective Fourier Transform for $\tau = 14,630$. A nanohole defectless pattern is obtained in the steady state.